Toxicology Reports 11 (2023) 116–128

Contents lists available at ScienceDirect

Toxicology Reports

journal homepage: www.elsevier.com/locate/toxrep

Subchronic pulmonary toxicity of ambient particles containing cement production–related elements

Eun-Jung Park [a,b,*,1], Mi-Jin Yang [c,1], Min-Sung Kang [c,d], Young-Min Jo [e], Cheolho Yoon [f], Yunseo Lee [a], Dong-Wan Kim [g], Gwang-Hee Lee [g], Ik-Hwan Kwon [h], Jin-Bae Kim [i]

[a] College of Medicine, Graduate School, Kyung Hee University, 02447, Republic of Korea
[b] Human Health and Environmental Toxins Research Center, Kyung Hee University, 02447, Republic of Korea
[c] Jeonbuk Branch Institute, Korea Institute of Toxicology, Jeongup 56212, Republic of Korea
[d] Department of Biomedical Science and Technology, Graduate school, Kyung Hee University, Seoul 02447, Republic of Korea
[e] Department of Environmental Science and Engineering, Global Campus, Kyung Hee University, Yongin 17104, Republic of Korea
[f] Ochang Center, Korea Basic Science Institute, Cheongju 28119, Republic of Korea
[g] School of Civil, Environmental and Architectural Engineering, Korea University, Seoul 02841, Republic of Korea
[h] Safety Measurement Institute, Korea Research Institute of Standards and Science, 34113, Republic of Korea
[i] School of Medicine, Kyung Hee University, Seoul, Republic of Korea

ARTICLE INFO

Handling Editor: Prof. L.H. Lash

Keywords:
Particulate materials
Cement
Pulmonary inflammation
Multinucleated macrophages
Autophagy

ABSTRACT

Chronic respiratory disease is among the most common non-communicable diseases, and particulate materials (PM) are a major risk factor. Meanwhile, evidence of the relationship between the physicochemical characteristics of PM and pulmonary toxicity mechanism is still limited. Here, we collected particles (CPM) from the air of a port city adjacent to a cement factory, and we found that the CPM contained various elements, including heavy metals (such as arsenic, thallium, barium, and zirconium) which are predicted to have originated from a cement plant adjacent to the sampling site. We also delivered the CPM intratracheally to mice for 13 weeks to investigate the pulmonary toxicity of inhaled CPM. CPM-induced chronic inflammatory lesions with an increased total number of cells in the lung of mice. Meanwhile, among inflammatory mediators measured in this study, levels of IL-1β, TNF-α, CXCL-1, and IFN-γ were elevated in the treated group compared with the controls. Considering that the alveolar macrophage (known as dust cell) is a professional phagocyte that is responsible for the clearance of PM from the respiratory surfaces, we also investigated cellular responses following exposure to CPM in MH-S cells, a mouse alveolar macrophage cell line. CPM inhibited cell proliferation and formed autophagosome-like vacuoles. Intracellular calcium accumulation and oxidative stress, and altered expression of pyrimidine metabolism- and olfactory transduction-related genes were observed in CPM-treated cells. More interestingly, type I-LC3B and full-length PARP proteins were not replenished in CPM-treated cells, and cell cycle changes, apoptotic and necrotic cell death, and caspase-3 cleavage were not significantly detected in cells exposed to CPM. Taken together, we conclude that dysfunction of alveolar macrophages may contribute to CPM-induced pulmonary inflammation. In addition, given the possible transformation of heart tissue observed in CPM-treated mice, we suggest that further study is needed to clarify the systemic pathological changes and the molecular mechanisms following chronic exposure to CPM.

1. Introduction

For the last few decades, adverse effects of ambient particulate materials (PM) on human health have been proven in numerous experimental and epidemiological studies. As a result, the World Health Organization (WHO) International Agency for Research on Cancer classified PM as a group 1 carcinogen (carcinogenic to humans) in 2013. Recent studies have also reported that outdoor air pollution contributed

* Correspondence to: Department of Biochemistry and Molecular Biology, Graduate School of Medicine, Kyung Hee University, Kyung Hee Daero 26, Dongdaemun-gu, Seoul 02447, Republic of Korea.
E-mail address: pejtoxic@khu.ac.kr (E.-J. Park).
[1] These authors contributed equally to this work as first authors.

https://doi.org/10.1016/j.toxrep.2023.07.002
Received 1 March 2023; Received in revised form 2 July 2023; Accepted 3 July 2023
Available online 7 July 2023

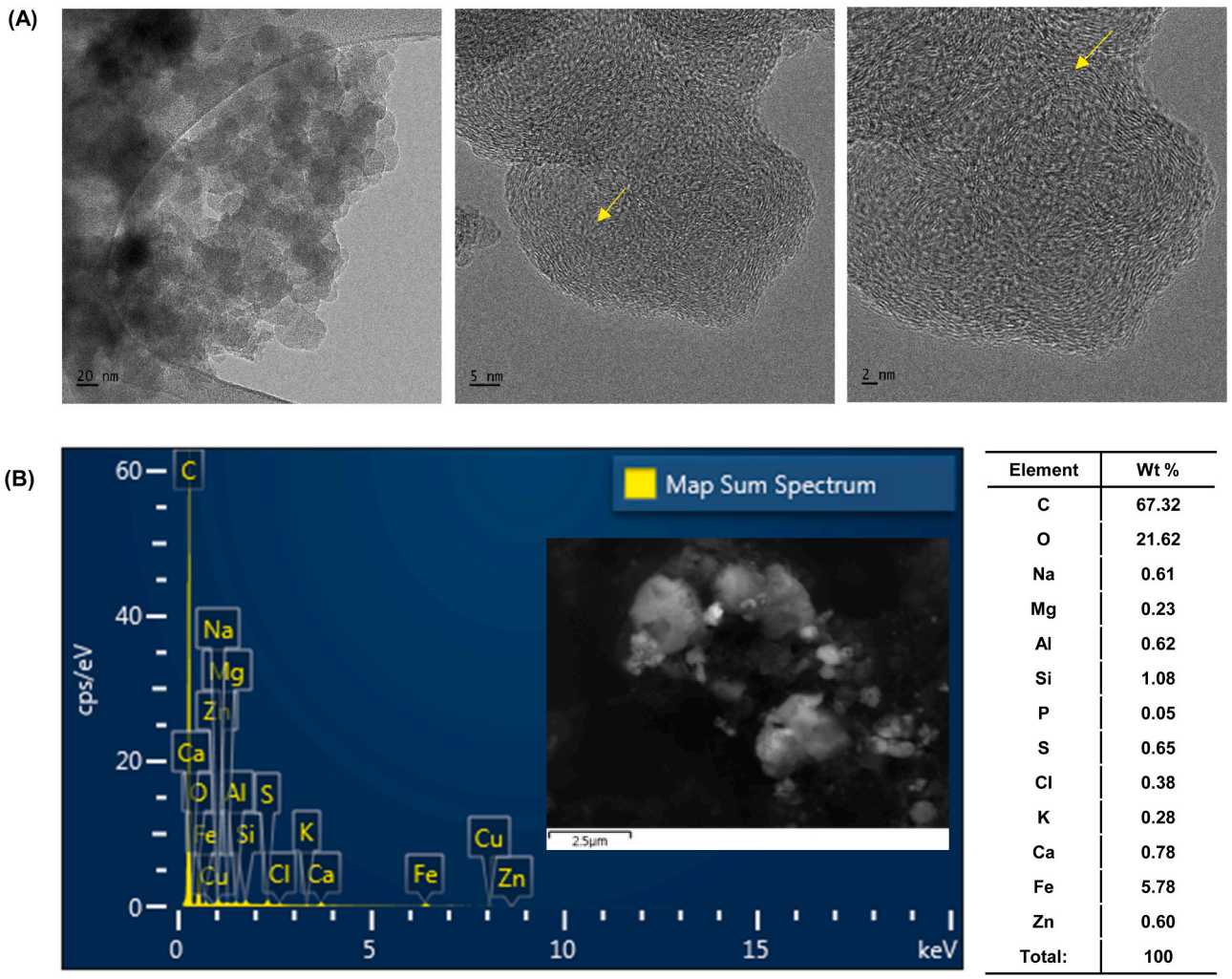

Element	Wt %
C	67.32
O	21.62
Na	0.61
Mg	0.23
Al	0.62
Si	1.08
P	0.05
S	0.65
Cl	0.38
K	0.28
Ca	0.78
Fe	5.78
Zn	0.60
Total:	100

Fig. 1. TEM (A) and EDX (B) images of CPM. Arrows point to graphite-like crystalline structures.

to approximately 9 million (1 in 6) deaths per year worldwide in 2019 [12] and that $PM_{2.5}$ (less than 2.5 μm in diameter) was largely responsible for the development of chronic diseases, including chronic obstructive and pulmonary disease, stroke, ischemic heart disease, lung cancer, and type 2 diabetes [11,37,6,8]. Similarly, chronic exposure to air pollutants can worsen existing respiratory diseases and increase the number of patients with decreased lung function [18,43,9]. Based on the accumulated scientific evidence, the WHO established new outdoor air-quality guidelines in 2021 [17]. However, global atmospheric monitoring network data shows that the air quality in most countries does not meet these guidelines, even in developed countries [6,32]. Furthermore, due to insufficient evidence on the relationship between the physicochemical characteristics of PM and the lung toxicity mechanism, there are still limitations in suggesting a strategy to prevent possible chronic lung diseases using atmospheric measurement data.

Carbon and silica are among the main components of PM, and they are mainly derived from fossil fuel consumption and the Earth's crust, respectively. In addition, a large number of organic and inorganic elements originating from natural and anthropogenic sources bind to the nucleated particles [7,23], and floating and resident populations, lifestyles, residential and industrial facilities, and traffic volumes have been known as important factors that depend on the characterization of PM [21]. For example, in a study using $PM_{2.5}$ collected from different sources (soil, urban, construction sites, coal-fired power plants, steel plants, and motor vehicle exhaust) in Laiwu, China [52], the level of iron and calcium was higher in urban and soil dust, and calcium, magnesium, and ammonium ions (NH_4^+) were more characteristic in construction-site dust. While iron, calcium, and sulfate ion (SO_4^{2-}) levels were higher in steel, organic, and elemental compounds, power-plant dust contained higher levels of SO_4^{2-}, aluminum, and NH_4^+. In addition, silica concentrations were higher in urban, soil, and motor-vehicle-exhaust dust samples, and more interestingly, the value of organic compounds (carbon components from vehicles and fires) and elemental compounds was higher in summer than in winter.

Accumulated evidence has demonstrated that the biodistribution and human health effects are closely related to the properties of PM, including composition, size, and shape [35,48,49]. In addition, structural and functional damage of organelles can be linked to cell damage, leading to inflammation and organ (or tissue) damage [38,41]. For example, as compared to PM of 13 different sizes (10 nm to 18 μm) collected in two cities in Switzerland and China [36], PM in Switzerland (Zürich) peaked at around 40 nm (23.3% of total PM mass), whereas around 0.75 μm (13.8–18.6%) and 4.23 μm (13.7–20.4%) particles were the most widely distributed forms of PM in China (Beijing). Also, the oxidative potential of PM from both regions clearly varied with size, depending on PM-borne metals. Considering that cement factories are one of the major sources of air pollutants that can threaten the respiratory health of residents [10,2,34], we here sampled particles (CPM) from the air of a port city adjacent to a cement factory. Then, we instilled the CPM to mice intratracheally for 13 weeks and identified the immunological and pathological changes in mice. Furthermore, we investigated the detailed cellular mechanism using alveolar macrophage

Table 1
Elements bound to CPM.

Elements	Li	Al	Ti	V	Cr	Mn	Fe	Co	Ni	Cu	Zn	As	Sr	Mo	Cd	Ba	Pb	Zr	Sb	Tl	Be	Ga	Rb
10 mg/mL (ppb)	47.9	47,371.5	667.3	198.8	245.0	1093.0	9028.7	14.2	174.7	202.6	810.6	762.4	488.0	148.1	5.9	1696.0	141.4	51.2	151.9	14.5	0.8	50.8	139.6

cells, known as dust cells.

2. Materials and methods

2.1. Sampling and analysis of CPM

CPM was sampled in winter (from December 2018 to February 2019) at Samcheok-si (Gangwon-do), a port city in Korea, using a quartz fiber filter (QR-100, Advantec Korea, Seoul, Korea), and a cement plant located at approximately 0.3 km from the sampling site. The filters were chopped with scissors and sonicated in autoclaved deionized water (DW). The DW containing the particles separated from the quartz fiber filter was lyophilized, resuspended in autoclaved DW, and filtered using a cell strainer (using a pore size of 100 μm followed by 40 μm). Freeze-drying, resuspension, and filtering were repeated once again, and finally, the dispersion (1 mg/mL) was autoclaved prior to the experiments. The morphology and hydrodynamic diameter of the CPM were analyzed using transmission electron microscopy (TEM, JEOL, JEM-2100 F, Japan) and a particle-size analyzer (ELSZ-1000, Photal Otsuka Electronics, Japan), respectively, and the particle-bound elements were analyzed using inductively coupled plasma mass spectrometry (ICP-MS, iCAP RQ, Thermo Fisher Scientific, Germany).

2.2. Animal management and intratracheal instillation

Specific-pathogen-free ICR male mice (6 weeks, 26–28 g, Orient Bio Inc., Seongnam, Korea) were housed at a relative humidity of 50% ± 20%, a temperature of 23 ± 3 ℃, 10–20 air changes/hour and a 12 h light/dark cycle for the whole experimental period. A commercial rodent diet (Nestle Purina, Gyeonggi-do, Korea) and autoclaved tap water were provided ad libitum. In our previous studies, inhaled subway dust induced the most severe inflammation at a concentration of 50 μg/mouse, but not 200 μg/mouse [29], inhaled PM10-induced inflammation also showed a tendency to reach a maximum at a concentration of 50 μg/mouse [31]. In this study, mice were mildly anesthetized by isoflurane inhalation (4%, Hana Pharm. Co. Ltd., Hwaseong-si, Gyeonggi-do, South Korea), and DW (50 μL for control) and the CPM (10, 25 and 50 μg in 50 μL DW) were delivered intratracheally to mice (weekly, 12 mice/group). Body weight was measured before treatment and at necropsy, and all test procedures were approved by the Kyung Hee University Institutional Animal Care and Use Committee (KHGASP-18–001) and carried out in accordance with the Guide for the Care and Use of Laboratory Animals, an Institute for Laboratory Animal Research publication.

2.3. Bronchoalveolar lavage cell analysis

The lungs (8 mice/group) were lavaged with autoclaved phosphate-buffered saline (PBS, 1.5 mL), and the bronchioalveolar lavage (BAL) fluids were separated into pellets (BAL cells) and supernatants by centrifugation. The BAL cells were re-suspended in PBS (200 μL), and the total number was counted under a phase contrast microscope (Olympus, Tokyo, Japan). The BAL cells (100 μL) were also mounted on a sliding glass by centrifugation (800 rpm) (Shandon Cytospin 4, Thermo Fisher Scientific Inc., Waltham, MA, USA), dipped in a Diff-Quik solution (Sysmex, Kobe, Japan) and classified as macrophages, neutrophils, lymphocytes, or eosinophils based on morphological characteristics (BX51, Olympus, Tokyo, Japan). In addition, the expression level of surface proteins on BAL cells and the composition of splenocytes were analyzed according to a protocol described in our previous study [29, 30].

2.4. Enzyme-linked immunosorbent assay

The supernatants obtained by centrifugation of BAL fluids were used to measure pulmonary levels of inflammatory mediators secreted into

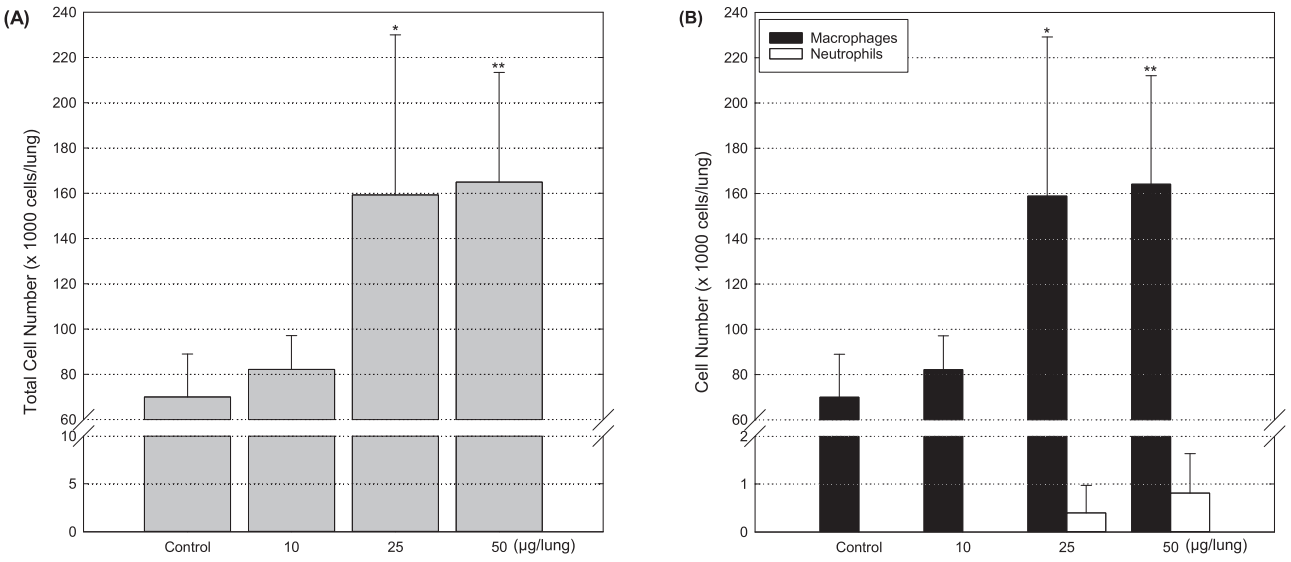

Fig. 2. Total number (A) and composition (B) of cells in the lungs of mice. BAL fluids (8 mice/group) were centrifuged, and the pellets were resuspended in a FACS buffer (200 μL). The cells were counted under a phase contrast microscope. Then, the part (100 μL) was mounted on the glass slide using cytospin, and 200 cells per sample were differentiated based on the morphological characterization. Data indicate the mean ± standard deviation (SD). $^{*}p < 0.05$, $^{**}p < 0.01$.

mice lungs, and the analysis was performed using anti-mouse enzyme-linked immunosorbent assay kits according to the manufacturer's instructions.

2.5. Histopathological examination

At necropsy, the lung, heart, thymus, and spleen (4 mice/group) were fixed in a 10% neutral-buffered formalin solution. The tissues were processed in the routine method using an automated instrument, and paraffin was then embedded into the tissues. The tissue samples were sectioned at a thickness of 3 μm and stained with a hematoxylin and eosin solution (Sigma-Aldrich, St. Louis, MO, USA). Histopathological differences between control and treated groups were examined under light microscopy (BX53, Olympus).

2.6. CPM uptake into alveolar macrophages

MH-S cells, a murine alveolar macrophage cell line (American Type Culture Collection, Manassas, VA, USA), were maintained in RPMI cell culture media containing 10% inactivated fetal bovine serum and 1% antibiotics (Thermo Fisher Scientific) at 37 °C in a 5% CO_2 humidified incubator. Alveolar macrophages work at an early stage after exposure to foreign particles. Additionally, a maximum of 50 μg per time was dosed to mice, and we used 1.5 mL per lung for BAL lavage. In this regard, the effect of CPM on cell viability was evaluated using a 3-(4,5-dimethylthiazol-2-yl)− 2,5-diphenyltetrazolium bromide solution as described previously [29]. CPM (a maximum concentration of 40 μg/mL) was exposed to MH-S cells for 24 h, and the cells were then fixed in primary and secondary fixing solutions, dehydrated, embedded in Spurr's resin, and placed for 24 h at 70 °C. Finally, morphological changes were observed using TEM (120 kV, Talos L120C, FEI, Czech).

2.7. Effects on structure and function of alveolar macrophages

A lactate dehydrogenase (LDH) assay kit (Cat No. K313, Biovision) was introduced to evaluate the effect of CPM on cell membrane integrity. MitoTracker Green FM (150 nM, Thermo Fisher Scientific), MitoTracker Red CMXRos (200 nM, Thermo Fisher Scientific) and adenosine triphosphate (ATP) assay kit (CellTiter-Glo 2.0, Promega, Fitchburg, WI, USA) were used to identify the effects of CPM on mitochondrial mass, mitochondrial membrane potential, and mitochondrial function, respectively. In addition, endoplasmic reticulum (ER) tracker Green (250 nM, Thermo Fisher Scientific), lysoTracker Green (50 nM, Thermo Fisher Scientific), and a neutral red assay kit (Cat No. K-447, BioVision) were used to assess the effect of CPM on ER volume, lysosomal structure, and lysosomal function, respectively. All experiments were performed according to the manufacturer's instructions.

2.8. Effects on intracellular free radical production

Intracellular reactive oxygen species (ROS) and reduced glutathione (GSH) levels were measured using carboxy-2′,7′-Dichlorofluorescein diacetate (Thermo Fisher Scientific) and a GSH assay kit (Cat No. K-261, BioVision, Milpitas, CA, USA), respectively, and extracellular nitric oxide (NO) level was measured using a NO assay kit (Cat No. 21023, iNtRON, Seongnam-si, Gyeonggi-do, Korea). All experiments were performed according to protocols suggested by the manufacturer.

2.9. Changes in gene expression profiles

To identify the effects of CPM on gene expression profile, we extracted total RNA from the control and treated (40 μg/mL) cells using TRIzol solution (FavorPrep Tri-RNA Reagent, Favorgen Biotech Corp., Ping-Tung, Taiwan) 24 h after treatment. Total RNA was quantified using a NanoDrop 2000 spectrophotometer (Thermo Scientific), and the effects of CPM on gene profiles were assessed using a GeneChip Mouse Gene 2.0 ST array at a specialized company (Macrogen Com.). Finally, gene-enrichment and functional annotation analysis for a significant probe list was performed using Gene Ontology (GO) (http://geneontology.org) and Kyoto Encyclopedia of Genes and Genomes (KEGG) (http://kegg.jp) databases.

2.10. Effects on protein expression

MH-S cells were incubated with CPM (0, 10, 20, and 40 μg/mL), and routine western blotting assays were performed using antibodies against the following: anti-SQSTM1/p62 and anti-caspase-1 mouse antibodies (Abcam, Cambridge, UK), anti-microtubule-associated protein 1 A/1B-light chain (LC)3B, anti-caspase-3, and anti-poly (ADP-ribose) polymerase (PARP) rabbit antibodies (Cell Signaling, Danvers, MA, USA), and anti-superoxide dismutase (SOD)− 1, anti-SOD-2, anti-interleukin (IL)− 18, or anti-β-actin antibodies (Santa Cruz Biotechnology, CA,

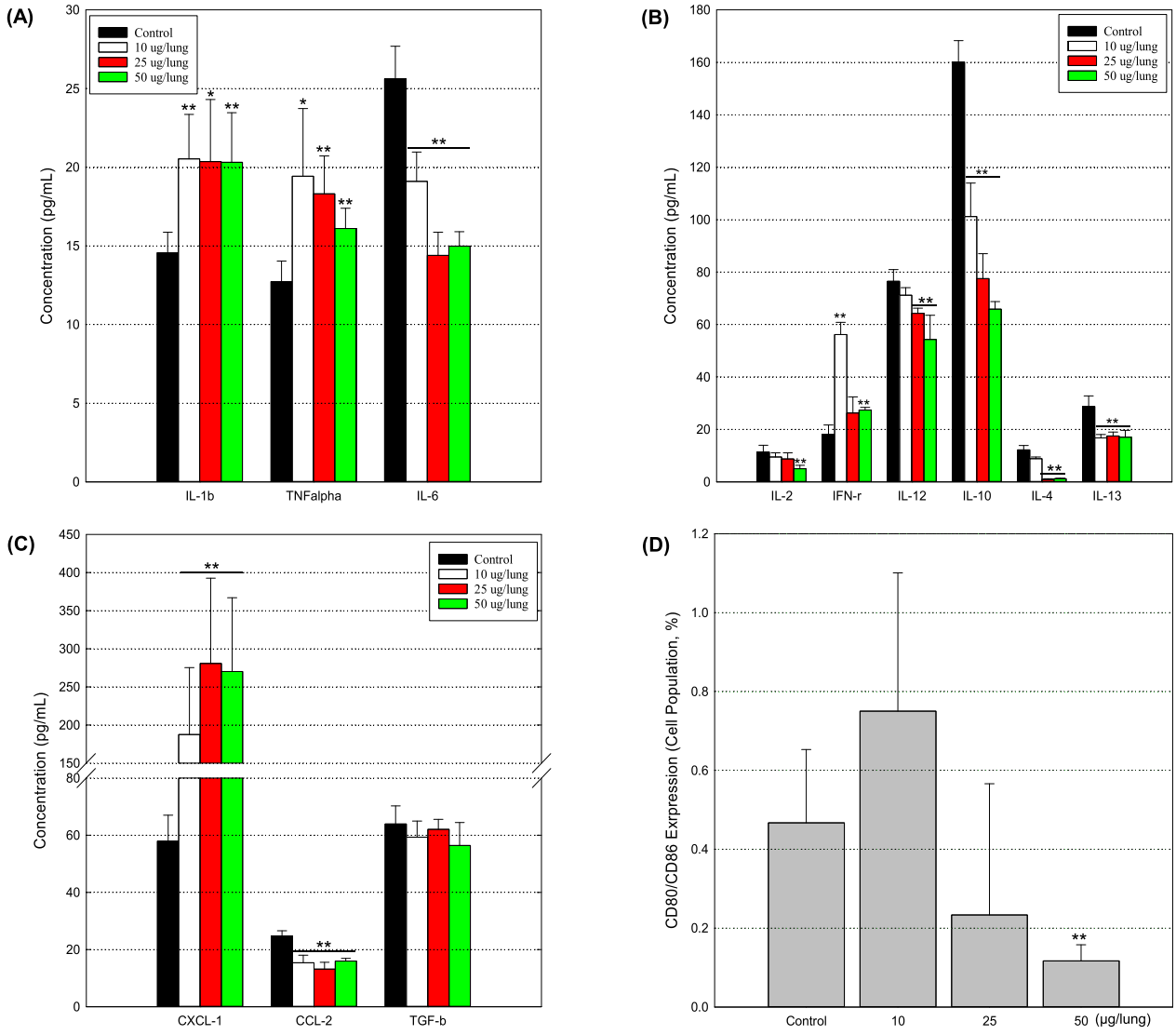

Fig. 3. Expression of inflammatory mediators following exposure to CPM. BAL fluids (8 mice/group) were separated into pellets and supernatants. The supernatants and a part of the pellets from two mice were pooled to make one sample for analysis. (N = 4 samples/group). *$p < 0.05$, * *$p < 0.01$. (A–C) The effects on both secretion of cytokines (or chemokines). (D) Co-expression of surface proteins (CD80 and CD86).

USA). Additionally, the cells were incubated with or without CPM (40 μg/mL) and fixed in a 4% paraformaldehyde solution and 100% methanol after 24 h of exposure. The cells were then blocked with 3% bovine serum albumin in PBS-containing 0.05% Tween-20 for 1 h at room temperature and incubated overnight at 4 ℃ with an anti-mouse β-actin antibody. After incubation with Alexa Fluor 488-conjugated anti-immunoglobin G antibodies (Molecular Probes), the cells were mounted using an aqueous mounting medium (Fluoroshield with DAPI, ImmunoBioScience Corp. Mukilteo, WA, USA) and visualized using a confocal laser scanning microscope (LSM710, Carl Zeiss, Germany).

2.11. Statistical analysis

Microarray data were analyzed using independent *t*-tests and fold changes, with a null hypothesis of no difference among groups. All data analysis and visualization of differentially expressed genes (DEGs) were performed using R3.3.2, and the false discovery rate was controlled by modifying the *p*-value using the Benjamini–Hochberg algorithm. For a DEG set, hierarchical cluster analysis was conducted using complete linkage and Euclidean distance as a measure of similarity. Gene-enrichment and functional annotation analysis for significant probe lists were processed using GO and KEGG pathway analyses. All other data were verified by Student's *t*-tests and one-way analysis of variance followed by Tukey's post hoc comparison (Prism9, GraphPad Software, San Diego, CA, USA).

3. Results

3.1. Characterization of CPM

The particles were amorphous (Fig. 1), and their average surface charge was about 24.9 ± 5.9 mV. The particle diameter was close to approximately 50 nm, whereas the average hydrodynamic diameter of the particles dispersed in DW was 969.8 ± 212.4 nm due to aggregation between particles (Supplementary Figure 1). Carbon accounted for approximately 67 wt% in dispersed CPM. We also found that CPM contained various elements, including arsenic, manganese, chrome, aluminum, iron, copper, and nickel (Table 1). Thallium, barium, and zirconium, which are closely related to cement manufacturing, were detected at significant levels.

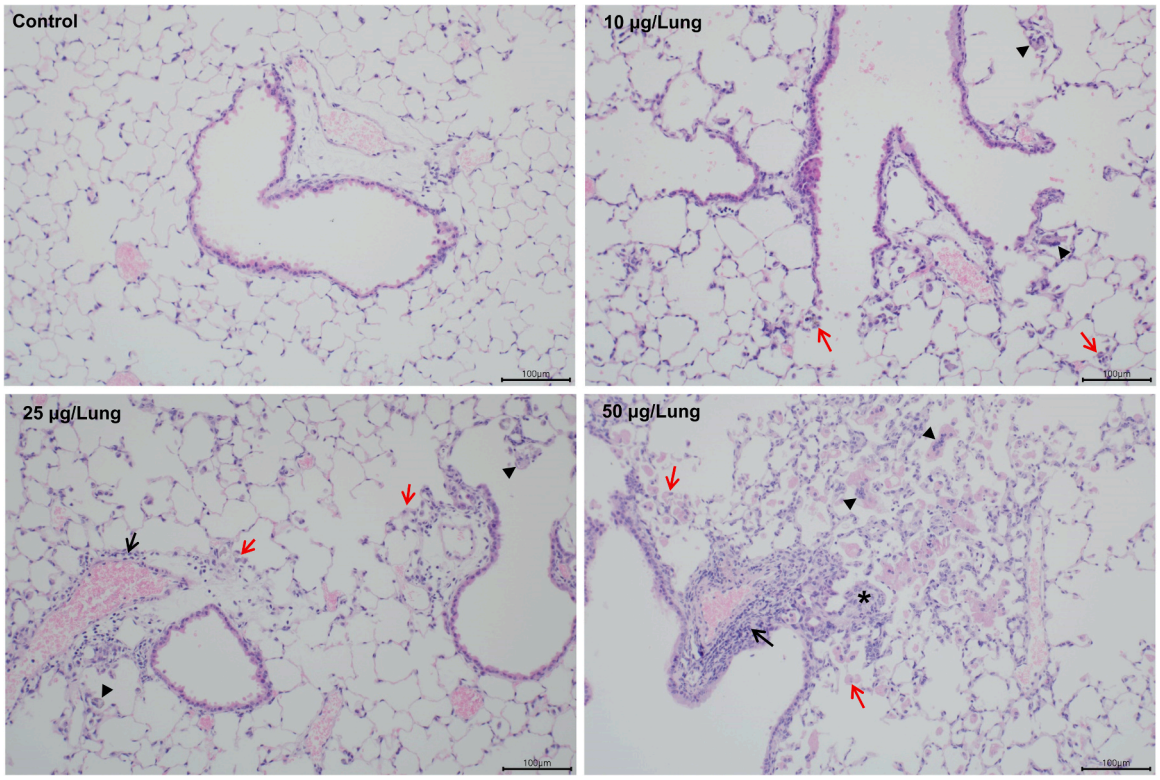

Fig. 4. Lung tissue damage following exposure to CPM. Four lung tissues per group were used for analysis, and representative images were suggested. Asterisk: thickened alveolar wall; triangle: multinucleated giant cells; black arrows: infiltration of inflammatory cells in perivascular; red arrows: aggregation of alveolar macrophages.

Table 2
A summary of pathological changes following exposure to CPM.

Tissues	Pathological changes	Control	10 μg/ lung	25 μg/ lung	50 μg/ lung
Lung	Aggregation, alveolar macrophage/ multinucleated giant cells	-	+ (2)	+ (4)	+ + (2), + (2)
	Infiltration, inflammatory cell, perivascular/interstitial	-	+ (1)	+ (4)	+ + (2), + (2)
	Thickened alveolar wall	-		+ (1)	+ (2)
	Mucous cell hyperplasia, bronchial epithelium	-		+ (1)	+ +(1)
Heart	-	-	-	-	-
Thymus	-	-	-	-	-
Spleen	-	-	-	-	-

Numbers in parentheses; Number of animals revealed the lesion. The severity of lesion; + (Mild), + + (Slight). '-': No significant pathological lesions.

3.2. Body weight changes

There were no significant differences in body weight gain between groups during the whole experimental period (Supplementary Figure 2). That of control mice was 17.2 ± 5.2 g, whereas the body weight gains of the treated mice were 17.7 ± 3.7 g, 18.9 ± 4.9 g, and 19.8 ± 4.9 g at doses of 10, 25, and 50 μg/mouse.

3.3. Increased pulmonary cell number

The total numbers of pulmonary cells were 85.6 ± 27.4, 100.0 ± 58.5, 167.9 ± 72.3 and 157.1 ± 50.2 (X 10^4) cells/lung in mice exposed to 0, 10, 25, and 50 μg of CPM, respectively (Fig. 2A). In addition, the total numbers of macrophages [167.9 ± 71.9 and 156.4 ± 49.8 (X 10^4) cells/lung, respectively] and neutrophils [0.4 ± 0.6 and 0.7 ± 0.9 (X 10^4) cells/lung, respectively] clearly increased in mice exposed to 25 and 50 μg of CPM compared with the control group (Fig. 2B). Meanwhile, there were no significant changes in the relative distribution of cell composition between groups, and lymphocytes and eosinophils were not detected in all the samples.

3.4. Altered pulmonary inflammatory mediators

In this study, we measured pulmonary levels of pro-inflammation (IL-1β, TNF-α, and IL-6)-, T cell growth stimulation (IL-2)-, helper 1 T cell differentiation (IL-12 and IFN-γ)-, helper 2 T cell differentiation (IL-10, IL-4, and IL-13)-, neutrophil chemotaxis (CXCL-1)-, monocyte chemotaxis (CCL-2)-, and anti-inflammation (TGF-β)-related inflammatory mediators. Very interestingly, among them, only levels of IL-1β, TNF-α, CXCL-1, and IFN-γ were elevated in the treated group compared with the controls. However, there were no dose-dependent effects (Fig. 3). Furthermore, the pulmonary level of IL-2, IL-4, IL-10, IL-12, IL-13, CCL-2, and TGF-β showed decreasing trends in mice exposed to CPM compared with the control mice. While the composition of lymphocytes in splenocytes did not show a difference between groups (Supplementary Figure 3), the BAL cells expressing antigen presentation–related proteins (CD80 and CD86) were remarkably reduced following exposure to CPM.

3.5. CPM persistence and tissue damage

The lung and heart are directly connected, and the thymus and spleen are lymphoid organs that control the functions of T cells and B cells, respectively, against foreign bodies. In this study, we investigated pathological lesions following exposure to CPM in these four tissues. We found aggregations of alveolar macrophages, formation of multinucleated giant cells, infiltration of inflammatory cells into the perivascular

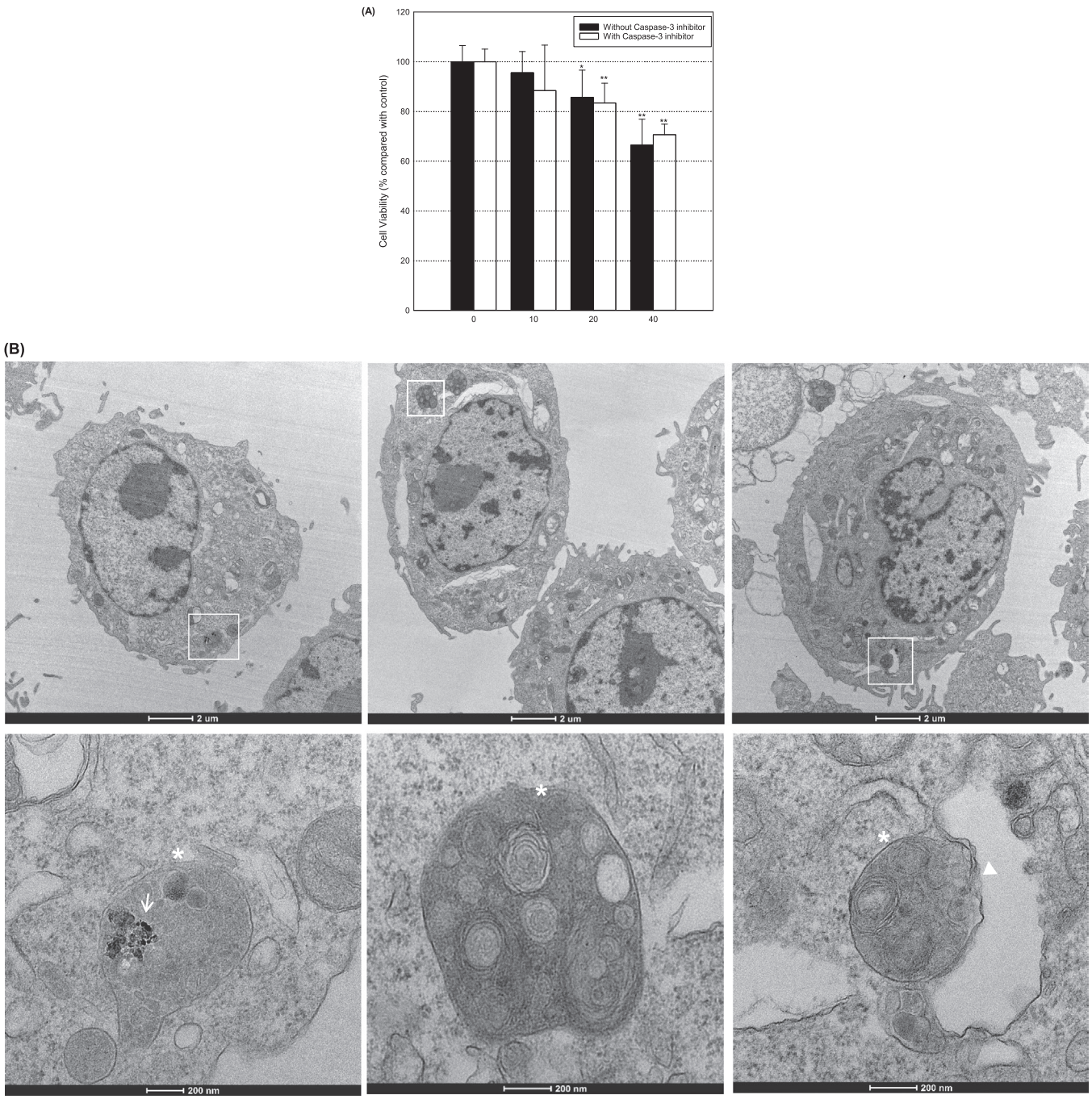

Fig. 5. Inhibition of cell proliferation (A) and formation of autophagosome (B) following exposure to CPM. Data show mean ± SD of six independent experiments (N = 6). *$p < 0.05$, * *$p < 0.01$. (A) MH-S cells (3 ×10^4 cells/mL) were exposed to CPM (0, 10, 20, and 40 μg/mL) for 24 h after pretreatment of z-VAD-fmk (20 μM, 30 min), a caspase-3 inhibitor, or without pretreatment. (B) MH-S cells were treated with 40 μg/mL of CPM for 24 h. White arrow: intracellular uptake of CPM; white asterisk: autophagosome; white triangle: the fusion between autophagosome and mitochondria.

and interstitial region, thickened alveolar walls, and mucous cell hyperplasia in bronchial epithelia in lungs from mice exposed to CPM for 13 weeks (Fig. 4, Table 2). However, there were no significant pathological changes in the heart, spleen, and thymus following exposure to CPM.

3.6. Cell proliferation inhibition

Alveolar macrophages are among representative cells in the first defense line against inhaled foreign particles, and aggregation of multinucleated alveolar macrophages was among the most notable pathological changes following exposure to CPM. Thus, we investigated cellular toxic responses of CPM using MH-S cells, a mouse alveolar macrophage cell line. Cell proliferation decreased in a dose-dependent manner after 24 h of exposure, and the level was 66.5% ± 8.6% of control at a concentration of 40 μg/mL (Fig. 5A). Meanwhile, as compared with the control, notable apoptotic and necrotic cell death were not observed in all the treated cells, cell cycles were not also distinctly different between groups (data not shown). Moreover, the decreased cell proliferation was not restored by co-treatment with an inhibitor of caspase-3, a hallmark of apoptosis (70.7% ± 3.5% of control at a concentration of 40 μg/mL). Meanwhile, importantly, vacuoles

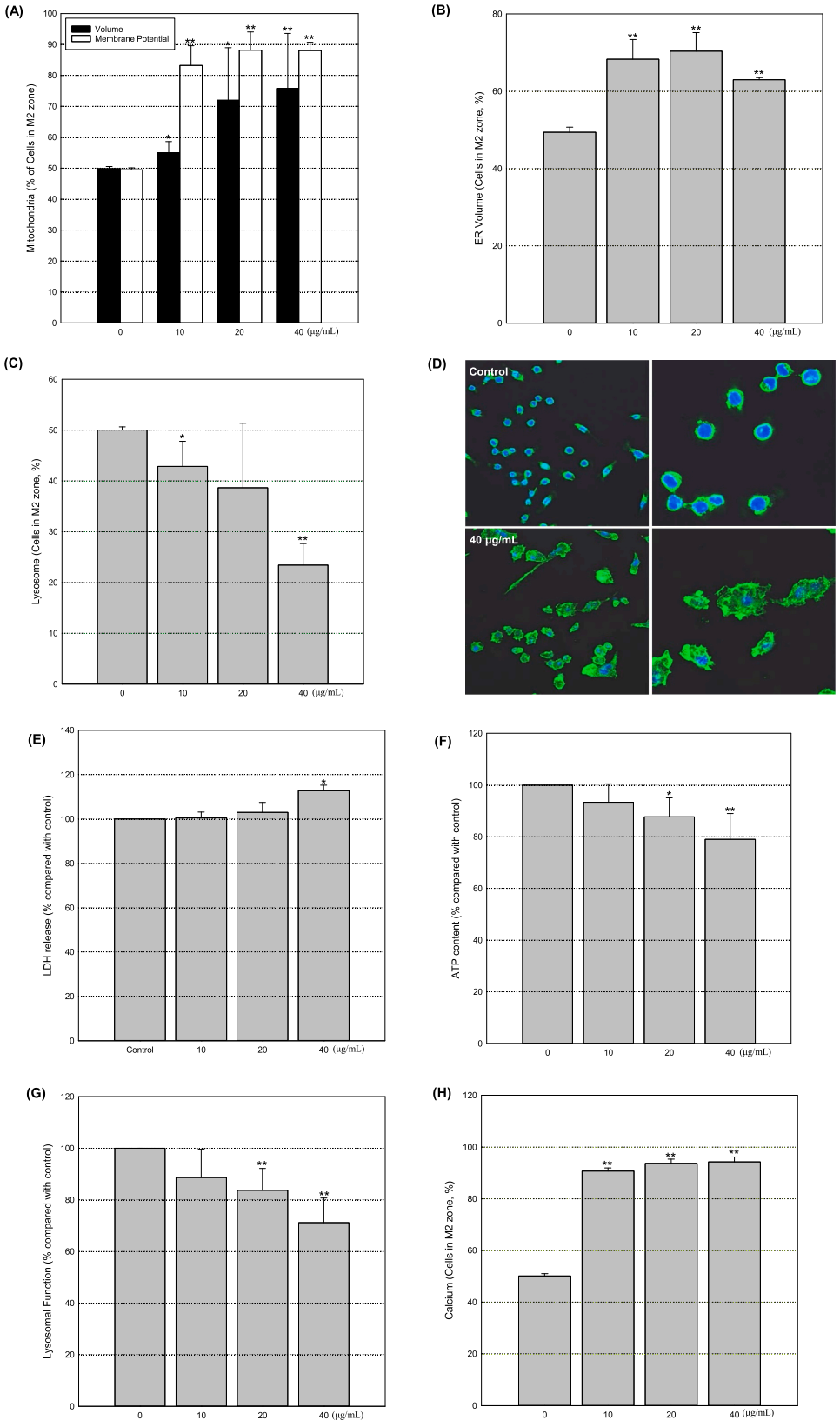

Fig. 6. Structural and functional damage of organelles following exposure to CPM. Effects of CPM on mass and membrane potential of mitochondria (A), ER volume (B), and lysosome structure (C). MH-S cells ($1x10^5$ cells/well) were stabilized in a 6-well plate and exposed to CPM (0, 10, 20, and 40 μg/mL) for 24 h. All the experiments were performed independently six times (mean ± SD, N = 6). $*p < 0.05$, $**p < 0.01$. (D) Distribution of β-actin protein. The cells (5000 cells/well) were stabilized overnight and treated with CPM (40 μg/mL) for 24 h. Effects of CPM on cell membrane integrity (E), ATP production (F), lysosomal function (G), and intracellular calcium accumulation (H). MH-S cells (3×10^4 cells/mL) were seeded and stabilized overnight. The cells were treated with a designated concentration of CPM for 24 h (N = 4). $*p < 0.05$, $**p < 0.01$.

containing CPM and impaired organelles were observed in the cytoplasm of cells harvested after 24 h of exposure, indicating the formation of autophagosome or autolysosome (Fig. 5B and Supplementary Figure 4). More interestingly, we could frequently find the opening of mitochondrial membranes and fusion between the mitochondria and the autolysosome under TEM, predicting mitophagy.

Structural and functional damage of cell components.

The mass of mitochondria (Fig. 6A) and ER (Fig. 6B) was extended in

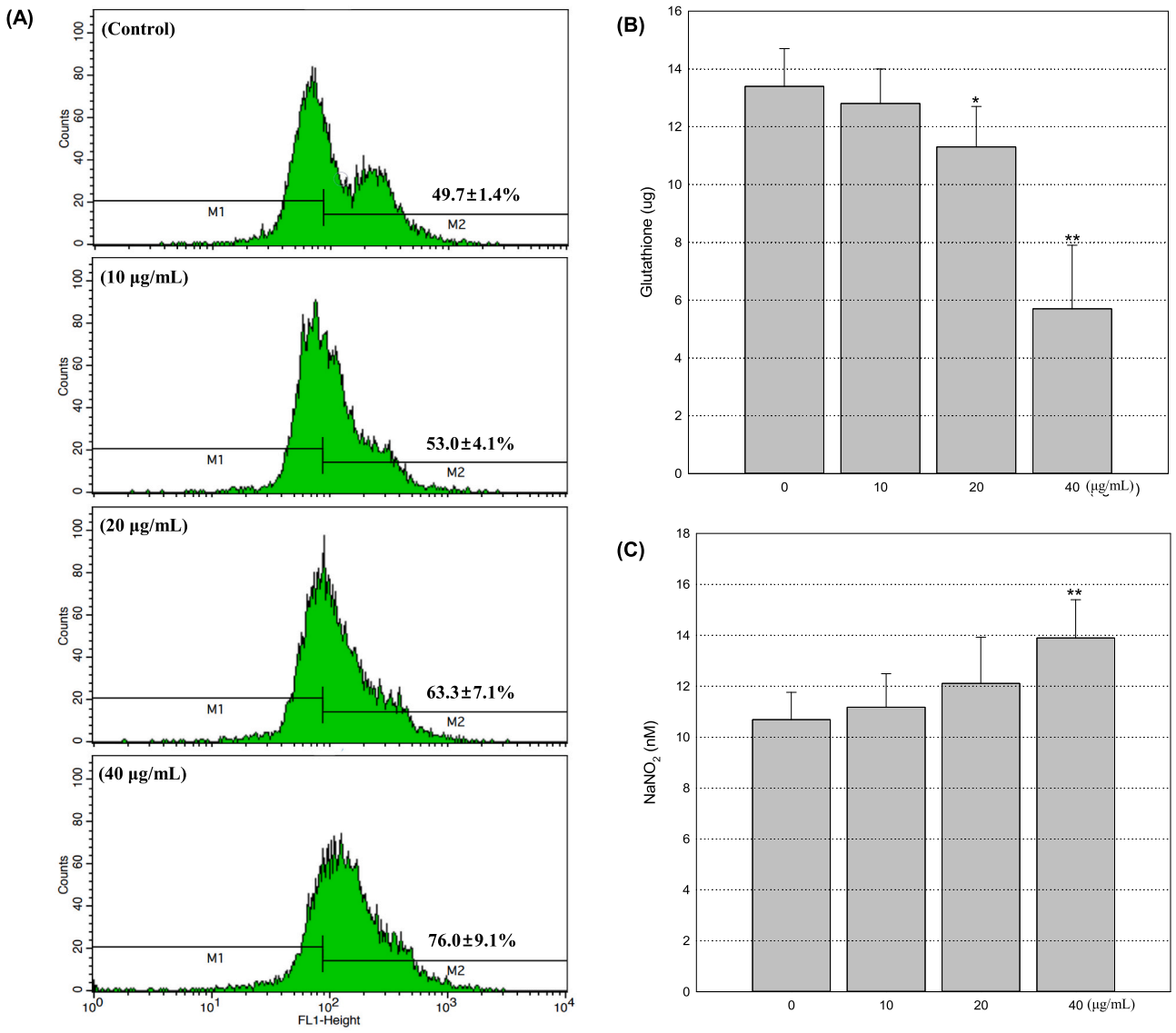

Fig. 7. Free radical production following exposure to CPM. *$p < 0.05$, * *$p < 0.01$. (A) ROS generation. MH-S cells (1×10^5 cells/well) were stabilized in a 6-well plate and exposed to CPM (0, 10, 20, and 40 μg/mL) for 24 h. The experiment was performed independently six times, and data are presented as the mean ± SD (N = 6). (B) Glutathione consumption. MH-S cells were harvested 24 h after treatment, and the lysates were reacted with NADPH. Data show mean ± SD of independent four experiments (N = 4). (C) NO production. MH-S cells ($1x10^6$ cells/well) were incubated with CPM (0, 10, 20, and 40 μg/mL) in a 12-well plate for 24 h. The experiment was performed independently six times (N = 6).

cells exposed to CPM compared with control, whereas lysosomes were shrunk with increasing concentrations (Fig. 6C). Intracellular distribution of β-actin was also changed remarkably in cells treated at the maximum concentration compared with controls (Fig. 6D). In addition, when treated for 24 h at a concentration of 40 μg/mL, the extracellular LDH level increased slightly compared with the control, indicating cell membrane damage (114.1% ± 1.7%) (Fig. 6E), whereas the uptake level of neutral red and the amount of produced ATP decreased significantly compared with the controls (80.5% ± 3.7% and 79.0% ± 10.0% of the control, respectively), showing dysfunction of lysosomes and mitochondria, respectively (Figs. 6F and 6G). More importantly, intracellular calcium accumulation (Fig. 6H) and mitochondrial membrane potentials (Fig. 6A) rapidly increased with CPM concentrations.

3.7. Oxidative stress

As shown in Fig. 7A, the intracellular ROS levels increased with concentrations, and levels of glutathione, an antioxidant, rapidly decreased with CPM concentrations (13.4 ± 1.3 μg and 5.7 ± 2.2 μg for control and 40 μg/mL of concentration, Fig. 7B). Similarly, the NO concentration in the cell culture media was 10.7 ± 1.1 and 13.9 ± 1.5 nmol in cells exposed to 0 and 40 μg/mL of CPM, respectively (Fig. 7C).

3.8. Altered gene expression

Table 3 shows changes in gene profiles following exposure to CPM. Interestingly, as compared differences between control cells and 40 μg/mL of CPM-treated cells, total 27 and 9 genes were significantly up- and down-regulated, respectively, and pyrimidine metabolism and olfactory transduction were most affected following exposure to CPM (Fig. 8).

3.9. Increased autophagy-related proteins

As shown in Fig. 8(D), conversion of LC3B from type I to type II, a representative indicator that suggests completion of the autophagosome, increased in CPM-treated cells accompanied by enhanced

Table 3
A gene list altered significantly following exposure to CPM (more than 1.5 fold).

Gene Description	mRNA Accession	Fold
Predicted gene 17079	XR_874617	2.15
MicroRNA 3094	NR_037277	2.02
	NONMMUT062770	2.00
Predicted gene, 24378 [Source:MGI Symbol; Acc:MGI:5454155]	ENSMUST00000122699	1.96
MicroRNA 1950	NR_035473	1.93
Zinc finger protein 97	NM_011765	1.89
Olfactory receptor 1431	NM_146414	1.89
Olfactory receptor 870	NM_146904	1.85
Predicted gene, 23205 [Source:MGI Symbol; Acc:MGI:5452982]	ENSMUST00000158671	1.79
Nuclear encoded rRNA 5 S 31 [Source:MGI Symbol;Acc:MGI:4421876]	ENSMUST00000104162	1.77
Predicted gene, 23303 [Source:MGI Symbol; Acc:MGI:5453080]	ENSMUST00000082714	1.76
Stefin A2	NM_001082545	1.76
Reproductive homeobox 3 F	NM_001040089	1.74
T cell receptor gamma joining 2	OTTMUST00000134814	1.73
Vomeronasal 1 receptor 72	NM_145843	1.66
Aly/REF export factor	NM_011568	1.66
Predicted gene, 22269 [Source:MGI Symbol; Acc:MGI:5452046]	ENSMUST00000104002	1.63
	NONMMUT051679	1.62
MicroRNA 30c-1	NR_029716	1.61
Predicted gene, 24145 [Source:MGI Symbol; Acc:MGI:5453922]	ENSMUST00000082631	1.61
Predicted gene, 24060 [Source:MGI Symbol; Acc:MGI:5453837]	ENSMUST00000157494	1.60
Predicted gene, 24174 [Source:MGI Symbol; Acc:MGI:5453951]	ENSMUST00000158933	1.60
Predicted gene, 23794 [Source:MGI Symbol; Acc:MGI:5453571]	ENSMUST00000084009	1.57
	NONMMUT042148	1.55
Predicted gene, 25183 [Source:MGI Symbol; Acc:MGI:5454960]	ENSMUST00000157752	1.55
Predicted gene, 22938 [Source:MGI Symbol; Acc:MGI:5452715]	ENSMUST00000103956	1.54
Vomeronasal 2, receptor, pseudogene 104 [Source:MGI Symbol;Acc:MGI:3761523]	ENSMUST00000099416	1.53
Nuclear encoded rRNA 5 S 200 [Source:MGI Symbol;Acc:MGI:4422065]	ENSMUST00000104194	1.52
Synovial sarcoma, X member B, breakpoint 1	NM_026492	1.50
Predicted gene, 25162 [Source:MGI Symbol; Acc:MGI:5454939]	ENSMUST00000158906	-1.51
Predicted gene, 22502 [Source:MGI Symbol; Acc:MGI:5452279]	ENSMUST00000082488	-1.51
Necdin	NM_010882	-1.51
Predicted gene 4858	NM_001034860	-1.52
Olfactory receptor 520	NM_147063	-1.53
Nuclear encoded rRNA 5 S 86 [Source:MGI Symbol;Acc:MGI:4421934]	ENSMUST00000083215	-1.54
RIKEN cDNA 4933402C06 gene	NR_045504	-1.54
Predicted gene, 25732 [Source:MGI Symbol; Acc:MGI:5455509]	ENSMUST00000175168	-1.58
Serine (or cysteine) peptidase inhibitor, clade A, member 1 C	NM_009245	-1.59
Olfactory receptor 1196	NM_146464	-1.60
Expressed sequence AA623943	XM_006534607	-1.63
Predicted gene, 25987 [Source:MGI Symbol; Acc:MGI:5455764]	ENSMUST00000083234	-1.69
Olfactory receptor 358	NM_207235	-1.73
	GENSCAN00000051494	-1.80

MH-S cells ($1X10^5$ cells/dish, 3 dishes/concentration/time) were stabilized overnight in 60 cm^2 cell culture dishes and incubated with or without CPM (40 μg/mL) for 24 h. Experiments were performed three times independently, and data are the mean ± SD.

expression of p62, a cargo protein. Expression of antioxidant proteins (SOD-1 and SOD-2), increased notably with concentration, and cleavage of PARP proteins, which contribute to repair of damaged DNA, increased with concentrations. Meanwhile, LC3B (type I) and total PARP proteins decreased following exposure to CPM. While expression of total caspase-3 protein increased, cleavage of caspase-3 (a final step of apoptosis) was not observed. Similarly, expression of caspase-1, an indicator for pyroptosis, was inhibited with CPM concentration.

4. Discussion

Quality control of environmental media, including air, water, and soil, along with individual lifestyle choices, is essential to maintaining and improving the health of local residents. Among them, the air quality policy is established based on scientific evidence from epidemiological studies that link the atmospheric concentration and the physicochemical properties of particulates with the health status of residents [11,33,6]. In addition, the physicochemical properties of PM have been regarded as key factors that determine the health effects of airborne contaminants. In our previous studies, we used particle samples collected from a building adjacent to a large apartment complex housing about 8000 people and a six-lane road in Seoul, the capital of Korea [30,31]. Meanwhile, in this study, CPM was collected from a rural area adjacent to the East Sea (approximately 0.3 km from the beach) and a train station (approximately 0.2 km) neighboring mountains. In 2018, the population and the population density were 68,326 and 57.52/km^2, respectively (Korean Statistical Information Service). Dump trucks frequently traveled through the area to transport cement from a nearby cement plant (approximately 0.3 km). We found that concentrations of arsenic, barium, and zirconium were significantly higher in the CPM (762.4, 1696.0, and 51.2 ppb, respectively) compared with the PM used in the previous study (20.67, 90.80, and 30.05 ppb, respectively) [30], and thallium was detected at a significant level in the current sample. Inhaled arsenic was closely associated with a high cancer risk among cement workers, as were silica and hexavalent chromium [20]. In addition, thallium can bind to particles during coal combustion and cement production [22], barium and zirconium have also been known to be applied in some cement manufacturing processes to improve the quality of concrete [1,50]. Furthermore, particle size is an important factor in determining lung burden and pulmonary distribution of PM [28,35,36]. As is well-known, inhalable particles less than 10 μm in diameter can reach into the alveolar region of the lungs, and some ultrafine particles (less than 0.1 μm in diameter) may travel throughout the body through the blood. In this study, the diameter of individual CPM was approximately 50 nm, whereas the average diameter of particles dispersed in DW reached approximately 1.0 μm due to aggregation (or agglomeration) between individual particles. Therefore, we hypothesize that CPM used in this study may translocate to the alveolar regions and deposit there, and that cement production–related chemicals may contribute, at least partially, to the toxicity identified in this study.

Inflammation is a series of defense responses that protect hosts against attacks from foreign bodies, and the host's cells may be damaged in this inflammatory response, ultimately leading to cell death. In addition, excessive inflammatory responses can cause tissue damage, resulting in an overload of dead cellular debris or damaged cells, and these unwanted cells can stimulate the host's immune system as well as foreign bodies. Similarly, inhaled toxicants can induce pulmonary inflammatory responses that have been linked to a variety of lung diseases, such as asthma, chronic obstructive pulmonary disease, idiopathic pulmonary fibrosis, and lung cancer [25,27,44,5], and numerous types of immune cells participate in this process via cytokines and chemokines. Additionally, because lungs are constantly exposed to foreign bodies, elaborate orchestration between cells that contribute to inflammation and anti-inflammation is essential for maintaining homeostasis between clearance of foreign bodies and tissue repair [45,46,48]. In this study, the total number of cells in the lungs of mice exposed to the maximum dose (50 μg/mouse) was about twice that of the control mice, but the composition did not differ significantly between groups. In addition, we found that secretion of innate immune response (IL-1β and CXCL-1), but not adaptive immune response–related mediators, increased in the lung of mice exposed repeatedly for 13 weeks. Similarly, although there were

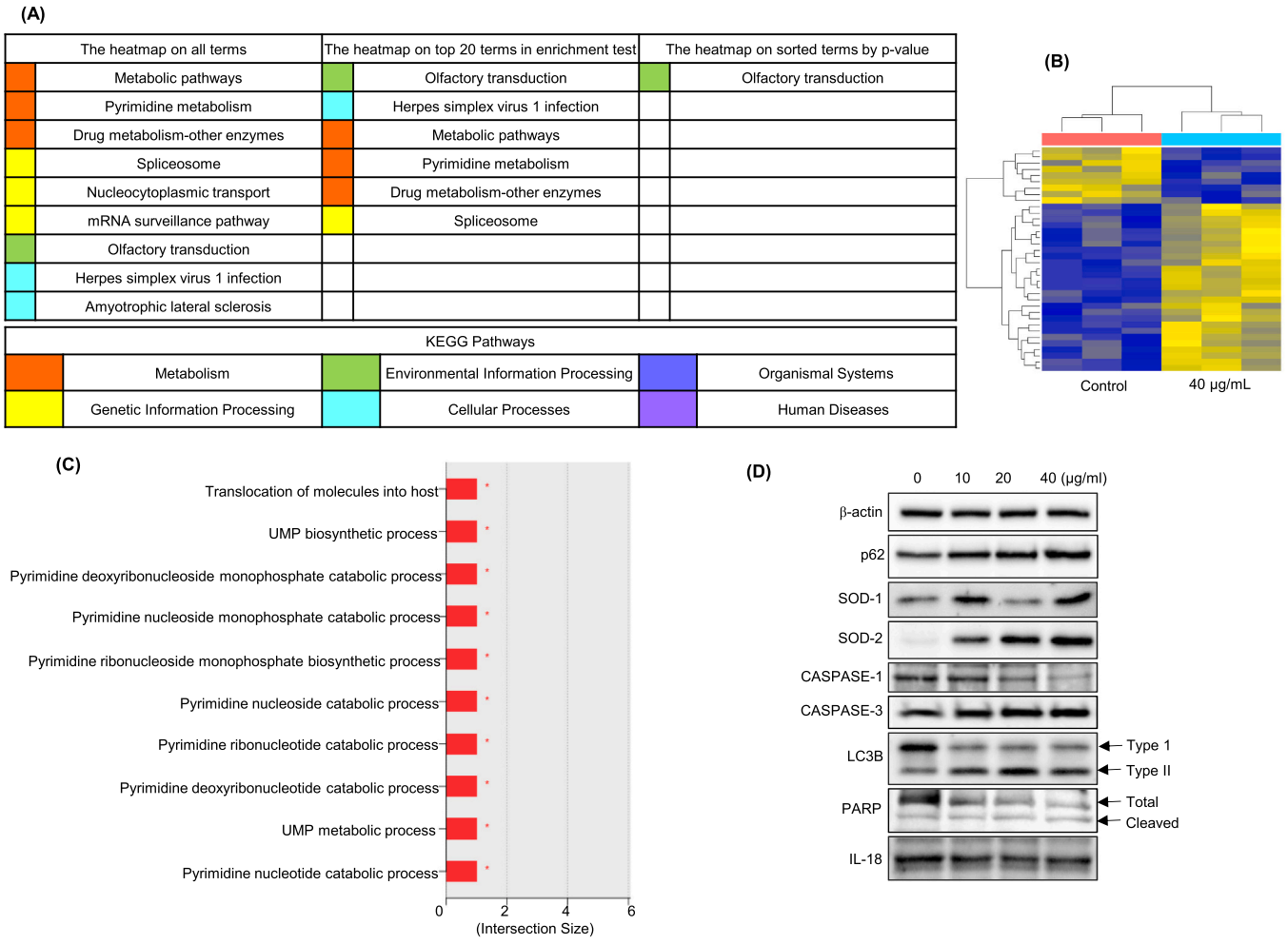

Fig. 8. Molecular changes following exposure to CPM. MH-S cells ($5x10^5$ cells/dish) were stabilized in 60 cm^2 of cell culture dishes and treated with CPM (0, 10, 20, and 40 μg/mL) for 24 h. Total RNA was extracted independently three times (9 dishes/group/time) for microarray analysis, and the difference in gene profile between control and treated cells (40 μg/mL) was analyzed. (A) KEGG enrichment heat map, (B) One-way hierarchical clustering heat map. An image was made using a Z-score of the normalized value. (C) Top 10 terms of GO functional analysis. (D) Changes in protein expression following exposure to CPM. MH-S cells ($5x10^6$ cells/dish) were stabilized in 100 cm^2 of cell culture dishes and treated with CPM (0, 10, 20, and 40 μg/mL) for 24 h. All the proteins were detected independently four times, and the representative data were presented. Each blot was quantified using the ImageJ program. $*p < 0.05$, $* *p < 0.01$.

no significant changes in the composition of lymphocytes, expression of surface proteins (CD80 and CD86) that play a central role in antigen presentation, was dramatically inhibited on the surface of BAL cells collected from the lungs of mice exposed to the highest doses of CPM. Furthermore, the lung supplies oxygen, which is essential for human life, and oxygen and carbon dioxide move between the capillaries and the walls of the alveoli under a concentration gradient. We can therefore expect that if the absolute area of the alveoli that oxygen can enter is reduced due to the inflow of foreign substances or infiltration of immune cells, or if the oxygen supply is defective due to poor flexibility of the alveolar wall, the efficiency of gas exchange between oxygen and carbon dioxide may decrease, resulting in hypoxia. In this study, we observed the infiltration of immune cells into the alveoli and thickened alveolar walls in the lungs of mice exposed to CPM. Therefore, we hypothesize that infiltration of immune cells into the alveoli may be attributable to low clearance of CPM and that chronic exposure to CPM may cause adverse health effects not only in the lungs but also systemically. In addition, arsenic, thallium, and barium are closely associated with the development of cardiovascular diseases [13,3,4,40], and we observed fibrotic tissues in the hearts of mice exposed to the maximum concentration of CPM (Supplementary Figure 5). Myocardial fibrosis can cause structural and electrical changes and provoke dysfunction of cardiac mechanics and arrhythmia [32]. In addition, mitochondrial damage, which can be caused by exposure to heavy metals, can lead to cardiac electrical instability by eliciting heterogeneity of the action potential of cardiomyocytes [5,47], and these changes can induce clinical arrhythmia, including atrial fibrillation or ventricular tachycardia [16,26]. Therefore, we suggest that further study is needed to clarify the possible systemic pathological changes and the molecular mechanisms following chronic exposure to CPM.

Pulmonary concentrations of inflammatory mediators are determined by various types of cells that make up the alveoli along with pulmonary immune cells, and alveolar macrophages are among the key players in triggering pulmonary inflammatory response against foreign bodies. In this study, multinucleated giant cells were observed in the lungs of mice exposed to CPM for 13 weeks, and damaged mitochondria, autophagosome formation, and persistence of particles within mitochondria or the cytoplasm were notably observed in TEM images of alveolar macrophages incubated with CPM (40 μg/mL) for 24 h, accompanied by structural and functional damage of mitochondria and cell proliferation inhibition. Distribution of β-actin protein was collapsed in CPM-treated alveolar macrophages, expression of p62 protein, a cargo protein, was remarkably enhanced, and LC3B protein was conversed from type-I to type-II (indicating completion of autophagosome). In addition, we found that intracellular calcium accumulation and oxidative stress were notable 24 h after CPM treatment. On

the other hand, very interestingly, type I-LC3B and full-length PARP proteins were not replenished in CPM-treated cells, and cell cycle changes, apoptotic and necrotic cell death, and caspase-3 cleavage were not significantly observed in cells exposed to CPM. In addition, among key indicators for pyroptosis, expression of only caspase-1 protein, but not IL-18 protein, dramatically decreased with CPM concentration. More interestingly, gene profile analysis showed that CPM most affected the expression of pyrimidine metabolism- and olfactory transduction-related genes. Furthermore, in the cytoplasm of human bronchial epithelial cells exposed to CPM for 24 h at 40 μg/mL, lysosomal membrane protein (LAMP-2) was aggregated, and a cis-Golgi membrane protein (GM-130) was dispersed (Supplementary Figure 6). The Golgi apparatus is a major collection and dispatch station of protein products received from the ER [51,54], and actin protein is a highly conserved protein that is involved in cell motility, structure, and integrity [15,24]. Additionally, impaired organelles are degraded in the autolysosome (fusion between autophagosomes and lysosomes) and then recycled within the cells or discarded by exocytosis. Intracellular calcium, ROS, and NO are secondary messengers that regulate intra- and extra-cellular signaling for cell proliferation, differentiation, and cellular motility [14, 42]. Moreover, cytosine, thymine, and uracil are pyrimidine derivatives that are essential components in nucleic acids, as well as purines, and pyrimidine derivatives are ultimately degraded to carbon dioxide, water, and urea [53]. Therefore, we hypothesize that CPM may cause adverse cellular responses by disturbing nucleic acid metabolism. In addition, the incidence of respiratory tract cancers (lung and bronchus cancer) was higher in Koreans living in the region adjacent to the cement plant compared with the common Koreans [10], and compared to workers in other occupations, cement plant workers had lower levels of respiratory health, showing an increase in adverse pulmonary symptoms and a decrease in lung function [2]. Furthermore, accumulated evidence suggests that competitive interference with potassium-dependent processes is a toxicity mechanism of thallium [13,27] and that barium can induce hypokalemia [19]. Potassium ions are a component of a wide variety of proteins and enzymes, influencing wide spectrums of physiological responses, and thus an imbalance of potassium ions can lead to dysfunction in neuronal, cardiac, and other systems, ultimately resulting in various diseases such as paresthesia and cardiac arrhythmias [39]. Herein, we propose that chronic toxicity of inhaled CPM, focusing on the possible contribution to the development of cardiovascular disease, should be performed to maintain the health of local residents.

In conclusion, we suggest that CPM-induced pulmonary inflammation may be associated with the dysfunction of alveolar macrophages that is attributable to dysregulation of crosstalk between autophagy (repair of damaged cells) and (apoptotic) cell death.

CRediT authorship contribution statement

Eun-Jung Park; Conceptualization, In vitro experiments, Draft writing, **Mi-Jin Yang**; Pathological analysis, Draft writing, **Min-Sung Kang**: Animal experiments, **Young-Min Jo**; Particle collection, **Cheolho Yoon**; ICP/MS analysis, **Yunseo Lee**; Draft writing, **Dong-Wan Kim, Gwang-Hee Lee**; Sample characterization, **Ik-Hwan Kwon**; Dark field image production, **Jin-Bae Kim**; Review, Editing.

Declaration of Competing Interest

The authors declare the following financial interests/personal relationships which may be considered as potential competing interests: Eun-Jung Park reports financial support was provided by Korea Environment Industry & Technology Institute.

Data Availability

The authors do not have permission to share data.

Acknowledgement

This research was supported by Korea Environment Industry & Technology Institute (KEITI Project No. 2022003310013).

Appendix A. Supporting information

Supplementary data associated with this article can be found in the online version at doi:10.1016/j.toxrep.2023.07.002.

References

[1] Al-Jadiri, R.S.F., et al., 2018. Producing a new type of cement by adding Zirconium Oxide. International Conference on Materials Engineering and Science. 454.
[2] Y.I. Al-Neaimi, et al., Respiratory illnesses and ventilatory function among workers at a cement factory in a rapidly developing country, Occup. Med. 51 (2001) 367–373.
[3] N.S. Alamolhodaei, et al., Arsenic cardiotoxicity: an overview, Environ. Toxicol. Pharmacol. 40 (2015) 1005–1014.
[4] B.S. Bhoelan, et al., Barium toxicity and the role of the potassium inward rectifier current, Clin. Toxicol. 52 (2014) 584–593.
[5] D.A. Brown, B. O'Rourke, Cardiac mitochondria and arrhythmias, Cardiovasc Res 88 (2010) 241–249.
[6] H. Carvalho, New WHO global air quality guidelines: more pressure on nations to reduce air pollution levels, Lancet Planet Health 5 (2021) e760–e761.
[7] J. Curtius, Nucleation of atmospheric aerosol particles, Comptes Rendus Phys. 7 (2006) 1027–1045.
[8] G.H. Dong, et al., Long-term exposure to ambient air pollution and respiratory disease mortality in Shenyang, China: a 12-year population-based retrospective cohort study, Respiration 84 (2012) 360–368.
[9] M. Elbarbary, et al., Ambient air pollution, lung function and COPD: cross-sectional analysis from the WHO Study of AGEing and adult health wave 1, BMJ Open Respir. Res (2020) 7.
[10] S.Y. Eom, et al., Increased incidence of respiratory tract cancers in people living near Portland cement plants in Korea, Int Arch. Occup. Environ. Health 90 (2017) 859–864.
[11] D. Evangelopoulos, et al., The role of burden of disease assessment in tracking progress towards achieving WHO global air quality guidelines, Int J. Public Health 65 (2020) 1455–1465.
[12] R. Fuller, et al., Pollution and health: a progress update, Lancet Planet Health 6 (2022) e535–e547.
[13] S. Galvan-Arzate, A. Santamaria, Thallium toxicity, Toxicol. Lett. 99 (1998) 1–13.
[14] A. Gorlach, et al., Calcium and ROS: a mutual interplay, Redox Biol. 6 (2015) 260–271.
[15] P.W. Gunning, et al., The evolution of compositionally and functionally distinct actin filaments, J. Cell Sci. 128 (2015) 2009–2019.
[16] S. Hamilton, et al., Sarcoplasmic reticulum-mitochondria communication; implications for cardiac arrhythmia, J. Mol. Cell Cardiol. 156 (2021) 105–113.
[17] B. Hoffmann, et al., WHO Air Quality Guidelines 2021-Aiming for Healthier Air for all: A Joint Statement by Medical, Public Health, Scientific Societies and Patient Representative Organisations. International Journal of Public Health, 2021, p. 66.
[18] X.Q. Jiang, et al., Air pollution and chronic airway diseases: what should people know and do? J. Thorac. Dis. 8 (2016) E31–E40.
[19] C.H. Johnson, V.J. VanTassell, Acute barium poisoning with respiratory failure and rhabdomyolysis, Ann. Emerg. Med 20 (1991) 1138–1142.
[20] N.H. Kamaludin, et al., Exposure to silica, arsenic, and chromium (VI) in cement workers: a probability health risk assessment. aerosol and air quality, Research 20 (2020) 2347–2370.
[21] F. Karagulian, et al., Contributions to cities' ambient particulate matter (PM): a systematic review of local source contributions at global level, Atmos. Environ. 120 (2015) 475–483.
[22] B. Karbowska, Presence of thallium in the environment: sources of contaminations, distribution and monitoring methods, Environ. Monit. Assess. 188 (2016) 640.
[23] M. Kulmala, et al., Measurement of the nucleation of atmospheric aerosol particles, Nat. Protoc. 7 (2012) 1651–1667.
[24] P. Lappalainen, et al., Biochemical and mechanical regulation of actin dynamics, Nat. Rev. Mol. Cell Biol. 23 (2022) 836–852.
[25] G.D. Leikauf, et al., Mechanisms of ultrafine particle-induced respiratory health effects, Exp. Mol. Med 52 (2020) 329–337.
[26] F.E. Mason, et al., Cellular and mitochondrial mechanisms of atrial fibrillation, Basic Res Cardiol. 115 (2020) 72.
[27] B. Moldoveanu, et al., Inflammatory mechanisms in the lung, J. Inflamm. Res 2 (2009) 1–11.
[28] G. Oberdorster, et al., Nanotoxicology: an emerging discipline evolving from studies of ultrafine particles, Environ. Health Perspect. 113 (2005) 823–839.
[29] E.J. Park, et al., Inhaled underground subway dusts may stimulate multiple pathways of cell death signals and disrupt immune balance, Environ. Res 191 (2020), 109839.
[30] E.J. Park, et al., PM 2.5 collected in a residential area induced Th1-type inflammatory responses with oxidative stress in mice, Environ. Res 111 (2011) 348–355.

[31] E.J. Park, et al., Effect of PM10 on pulmonary immune response and fetus development, Toxicol. Lett. 339 (2021) 1–11.
[32] R. Perez Velasco, D. Jarosinska, Update of the WHO global air quality guidelines: systematic reviews - an introduction, Environ. Int 170 (2022), 107556.
[33] O. Raaschou-Nielsen, et al., Particulate matter air pollution components and risk for lung cancer, Environ. Int 87 (2016) 66–73.
[34] E. Raffetti, et al., Cement plant emissions and health effects in the general population: a systematic review, Chemosphere 218 (2019) 211–222.
[35] M. Riediker, et al., Particle toxicology and health - where are we? Part Fibre Toxicol. 16 (2019) 19.
[36] I. Salma, et al., Lung burden and deposition distribution of inhaled atmospheric urban ultrafine particles as the first step in their health risk assessment, Atmos. Environ. 104 (2015) 39–49.
[37] S. Sang, et al., The global burden of disease attributable to ambient fine particulate matter in 204 countries and territories, 1990-2019: A systematic analysis of the Global Burden of Disease Study 2019, Ecotoxicol. Environ. Saf. 238 (2022), 113588.
[38] R. Sivacoumar, et al., Particulate matter from stone crushing industry: size distribution and health effects, J. Environ. Eng. 132 (2006) 405–414.
[39] C. Tian, et al., Potassium channels: structures, diseases, and modulators, Chem. Biol. Drug Des. 83 (2014) 1–26.
[40] V.P. Vineetha, K.G. Raghu, An overview on arsenic trioxide-induced cardiotoxicity, Cardiovasc. Toxicol. 19 (2019) 105–119.
[41] Y. Wang, et al., Urban particulate matter disturbs the equilibrium of mitochondrial dynamics and biogenesis in human vascular endothelial cells, Environ. Pollut. 264 (2020), 114639.
[42] Y. Wang, et al., Ambient particulate matter triggers dysfunction of subcellular structures and endothelial cell apoptosis through disruption of redox equilibrium and calcium homeostasis (vol 394, 122439, 2020), J. Hazard. Mater. (2021) 402.
[43] E.M. Wong, et al., Ultrafine particulate matter combined with ozone exacerbates lung injury in mature adult rats with cardiovascular disease, Toxicol. Sci. 163 (2018) 140–151.
[44] T. Xia, et al., Impairment of mitochondrial function by particulate matter (PM) and their toxic components: implications for PM-induced cardiovascular and lung disease, Front Biosci. 12 (2007) 1238–1246.
[45] Y.F. Xing, et al., The impact of PM2.5 on the human respiratory system, J. Thorac. Dis. 8 (2016). E69-74.
[46] M. Yamada, et al., Inflammatory responses in the initiation of lung repair and regeneration: their role in stimulating lung resident stem cells, Inflamm. Regen. 36 (2016) 15.
[47] K.C. Yang, et al., Mitochondria and arrhythmias, Free Radic. Biol. Med 71 (2014) 351–361.
[48] L. Yang, et al., The impact of PM(2.5) on the host defense of respiratory system, Front Cell Dev. Biol. 8 (2020) 91.
[49] Y. Yue, et al., Size-resolved endotoxin and oxidative potential of ambient particles in Beijing and Zurich, Environ. Sci. Technol. 52 (2018) 6816–6824.
[50] A. Zezulova, et al., The influence of barium sulphate and barium carbonate on the Portland cement, Ecol. N. Build. Mater. Prod. 151 (2016) 42–49, 2016.
[51] C.H. Zhang, et al., GM130, a cis-Golgi protein, regulates meiotic spindle assembly and asymmetric division in mouse oocyte, Cell Cycle 10 (2011) 1861–1870.
[52] G.Q. Zhang, et al., Chemical compositions and sources contribution of atmospheric particles at a typical steel industrial urban site, Sci. Rep. (2020) 10.
[53] Y. Zhang, et al., Uridine metabolism and its role in glucose, lipid, and amino acid homeostasis, Biomed. Res Int 2020 (2020) 7091718.
[54] Y.J. Zhang, et al., Golgi stress response, hydrogen sulfide metabolism, and intracellular calcium homeostasis, Antioxid. Redox Signal. 32 (2020) 583–601.